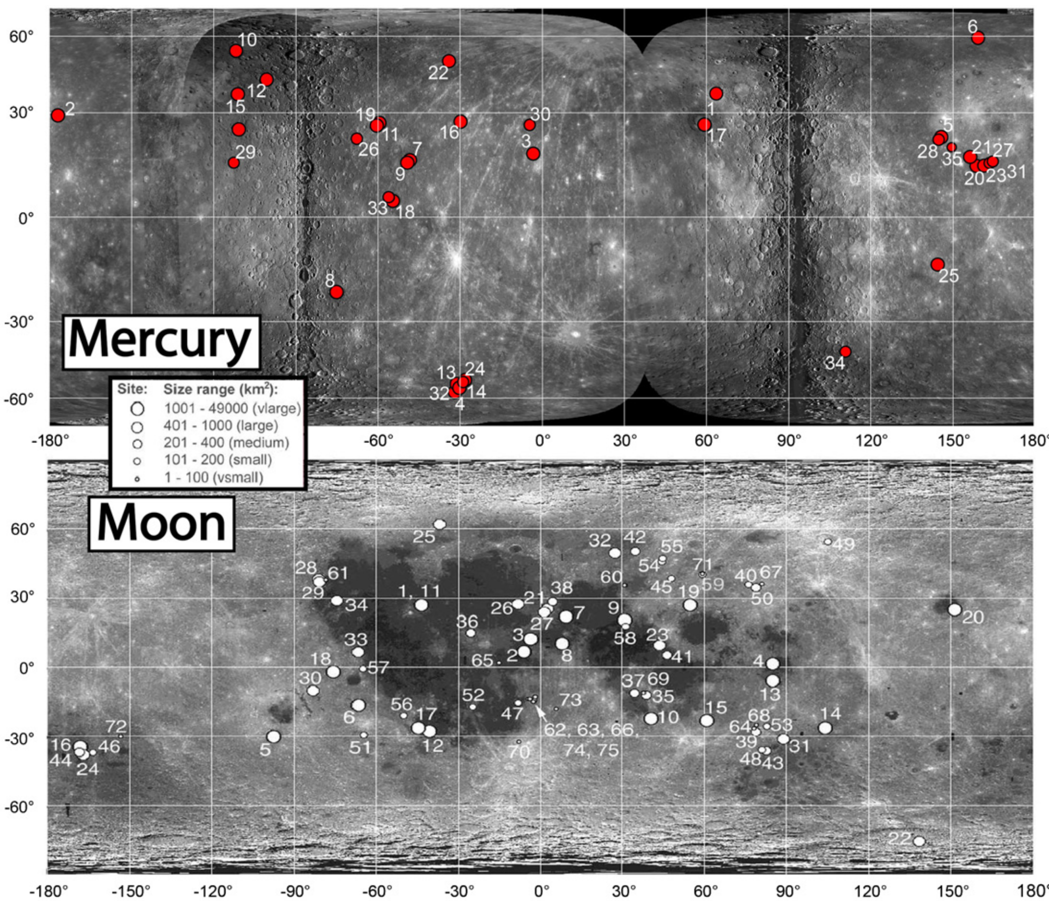

Fig. 4. Global distribution of candidate pyroclastic deposits on Mercury compared with those on the Moon (from Gaddis et al., 2003) using the same schematic representation. Deposits on each body are numbered in order of decreasing size (1 is the largest). The mercurian deposits are referenced by number in Table 1. The lunar deposits are referenced by number in Table 1 of Gaddis et al. (2003). Whereas lunar pyroclastic deposits tend to cluster near mare deposits, mercurian pyroclastic deposits are more widely distributed. There is a clustering of deposits at the edges of the Caloris basin, which is partially filled with volcanic material (Head et al., 2008; Murchie et al., 2008). The background image of the Moon (Gaddis et al., 2003) is the global 750-nm Clementine mosaic. The background image for Mercury is the 750-nm MESSENGER NAC mosaic from flybys 1, 2, and 3 (Becker et al., 2009). Some clustering in the Mercury distribution is likely to be a consequence of variations in viewing angle and incidence angle affecting the identification of pyroclastic features, as depicted in Fig. 1.

deposits on Mercury occur in a variety of geographical locations and are often located on crater floors. Unlike many pyroclastic deposits on the Moon (Gaddis et al., 2003), pyroclastic deposits on Mercury do not appear to be associated with floor-fractured craters, though they can be associated with crater peak rings.

The distribution of pyroclastic deposits on Mercury may suggest a more even distribution of heat-producing elements or interior volatiles, or a more uniform crustal thickness, each of which might allow magma to form and propagate to the surface with a more widespread distribution than seen on the Moon. Alternatively, the different spatial distribution of basins may exert a control on the distribution of pyroclastic deposits on the Moon and Mercury. The apparently more widespread and more global distribution of plains on Mercury relative to the Moon (e.g., Head et al., 2008; Denevi et al., 2009) may also be associated with this difference.

2.4. *Physical properties*

The area and the average radius were measured for each candidate pyroclastic deposit. NAC and WAC image mosaics (Becker et al., 2009) were placed onto an azimuthal-equidistant projection centered on the deposit being measured. Areas were calculated using ArcGIS, a geographic information system software package, by defining the edges of each feature. Radii were determined by averaging 12 transects from the center of the candidate vent (or the approximate center of the deposit in cases where a vent was not obvious) to the edge of the deposit (Table 1). For this reason, size rankings according to area are not always the same as size rankings according to average radius, depending on the irregularity of the deposit and the location of the features interpreted to be vents (Table 1). Because the edges of pyroclastic deposits are commonly diffuse, radius measurements are approximate and can be uncertain by up to several kilometers. Deposit edges were determined using a combination of albedo variations in the 500 m/pixel NAC monochrome image mosaic supplemented by ∼5 km/pixel WAC color boundaries. Due to the lower resolution of WAC images, NAC albedo variations were usually more precise, except for areas where lighting or viewing geometry was not ideal. Some of the large, broad, diffuse deposits lacked a coherent shape or a visible vent. The measured radii are least accurate for these deposits, as they could be composed of several overlapping deposits from different vents. Because of poor image quality in the vicinity of unnamed crater 4 (Fig. 2d), this deposit was not measured. Radii calculated from the area (under the assumption that each deposit is circular in extent) result in radii equal to (when the vent is nearly circular) or larger than (when the vent is highly irregular) radii directly measured and averaged from the images. Features were classified as "very large (1001–49,000 km^2)," "large (401–1000 km^2)," "medium (201–400 km^2)," "small (101–200 km^2)," and "very small (1–100 km^2)" according to the size classification used by Gaddis et al. (2003) for the Moon (shown in Fig. 4). The measured radii were tabulated, and a graphical representation of these results is